

# DEFA: Efficient Deformable Attention Acceleration via Pruning-Assisted Grid-Sampling and Multi-Scale Parallel Processing

Yansong Xu<sup>1</sup>, Dongxu Lyu<sup>1</sup>, Zhenyu Li<sup>1</sup>, Zilong Wang<sup>1</sup>, Yuzhou Chen<sup>1</sup>, Gang Wang<sup>1</sup>, Zhican Wang<sup>1</sup>,  
Haomin Li<sup>1</sup>, Guanghui He<sup>1,2\*</sup>

<sup>1</sup>School of Electronic Information and Electrical Engineering, Shanghai Jiao Tong University, Shanghai, China

<sup>2</sup>MoE Key Lab of Artificial Intelligence, AI Institute, Shanghai Jiao Tong University, China

{xys-13,lvdongxu,ambitious-lzy,wangzilongsjtu,huygens,wangganganjstu,guanghui.he}@sjtu.edu.cn

## ABSTRACT

Multi-scale deformable attention (MSDeformAttn) has emerged as a key mechanism in various vision tasks, demonstrating explicit superiority attributed to multi-scale grid-sampling. However, this newly introduced operator incurs irregular data access and enormous memory requirement, leading to severe PE under-utilization. Meanwhile, existing approaches for attention acceleration cannot be directly applied to MSDeformAttn due to lack of support for this distinct procedure. Therefore, we propose a dedicated algorithm-architecture co-design dubbed DEFA, the first-of-its-kind method for MSDeformAttn acceleration. At the algorithm level, DEFA adopts frequency-weighted pruning and probability-aware pruning for feature maps and sampling points respectively, alleviating the memory footprint by over 80%. At the architecture level, it explores the multi-scale parallelism to boost the throughput significantly and further reduces the memory access via fine-grained layer fusion and feature map reusing. Extensively evaluated on representative benchmarks, DEFA achieves 10.1-31.9 $\times$  speedup and 20.3-37.7 $\times$  energy efficiency boost compared to powerful GPUs. It also rivals the related accelerators by 2.2-3.7 $\times$  energy efficiency improvement while providing pioneering support for MSDeformAttn.

## KEYWORDS

Transformer, Deformable Attention, Pruning, Domain-Specific Acceleration, Grid-Sampling

## 1 INTRODUCTION

DEtection TRansformer (DETR) has gained increasing popularity in object detection due to the promising performance from the end-to-end optimizable network architecture. Recently, multi-scale deformable attention (MSDeformAttn) [1], inspired by deformable convolution (DeformConv) [2], is proposed to further improve the DETR resolution on small objects with linear complexity, which only samples a small set of key points from multi-scale feature maps (fmaps) instead of traversing across all of them via  $O(n^2)$ -level  $Q \times K^T$  in traditional attention [3]. Benefiting from multi-scale grid-sampling (MSGs), Deformable DETR achieves state-of-the-art detection accuracy so that MSDeformAttn has been widely adopted in recent 2D [4, 5, 1] and 3D [6, 7, 8] object detection networks.

However, MSDeformAttn suffers from significant computation inefficiency on general-purpose platforms such as CPUs and GPUs. For instance, Deformable DETR (173GFLOPs) [1] executes at only

9.7fps even on a powerful Nvidia RTX 3090Ti GPU, while Faster R-CNN[9] with a similar workload (180GFLOPs) can reach over 25fps for the same task. With our deep analysis, MSDeformAttn takes up to 54.7% of end-to-end inference latency while the MSGS procedure dominates (over 60%) within each attention layer, which becomes the major efficiency bottleneck. Suffering from the dynamically unordered and unbounded sampling candidates all over the feature maps, grid-sampling results in heavily irregular memory access and high cache miss rate, further leading to severe PE under-utilization on GPUs. In addition, applying multi-scale feature maps increases both the number of sampling points and the size of sampled fmaps by 21.3 $\times$  compared to using single-scale ones, exacerbating the intensity of memory footprint.

Domain-specific accelerator (DSA) is an effective solution to improve the processing efficiency on resource-limited terminals. Many existing DSAs [10, 11, 12] have been proposed to optimize attention [3] via reducing redundant computation between weak-related tokens. Nevertheless, MSDeformAttn reconstructs vastly different attention pipelines based on MSGS so that these works cannot maintain the superiority of MSDeformAttn due to a lack of support for grid-sample. Although some works [13, 14] also enhance similar grid-sample-based operators like deformable convolution[2], their methods, especially the aggressive sampling range restriction induce unacceptable accuracy loss and also cannot be applied to MSDeformAttn dataflow directly.

Therefore, we propose **DEFA**, a dedicated MSDeformAttn accelerator with algorithm-architecture co-optimization. The main contributions are as follows:

- (1) We comprehensively characterize the performance bottlenecks of MSDeformAttn in deformable transformers and identify the root cause of deployment inefficiency.
- (2) At the algorithm level, we propose a pruning-assisted grid-sampling scheme by deeply exploiting the sampling redundancy. To reduce the memory access of sampled fmaps, frequency-weighted fmap pruning (FWP) is adopted to ignore 43% unimportant pixels based on inter-layer pixel-wise acquisition. Meanwhile, probability-aware point pruning (PAP) is also applied to achieve an 84% reduction in memory access through softmax-based sparsity exploitation.
- (3) At the hardware level, we design an efficient MSDeformAttn architecture while fully harnessing the performance gains from algorithm-level optimization. we decouple the intra-level sampling computation to explore the multi-scale parallelism for bank conflict elimination, boosting the MSGS

\*Corresponding author: Guanghui He.

throughput by 3.06×. Furthermore, fine-grained operator fusion is adopted within each MSDeformAttn layer to avoid heavy data movement between sample and aggregation, which benefits from a reconfigurable PE array for MSGS and matrix computation.

- (4) Implemented on 40nm technology and extensively evaluated on representative benchmarks, MSDeformAttn achieves up to 10.1-31.9× speedup and 20.3-37.7× energy efficiency improvement over Nvidia RTX 2080Ti & 3090Ti GPUs. Compared with the related accelerators, it improves the energy efficiency by 2.2-3.7×, while supporting MSDeformAttn.

## 2 PRELIMINARY

### 2.1 Multi-Scale Deformable Attention

MSDeformAttn identifies relations between each query and a small set of sampling points in multi-scale fmaps  $X \in \mathbb{R}^{N_{in} \times D_{in}}$ . Let  $N_{in}$  and  $D_{in}$  denote the length of flattened feature maps from  $N_l$  levels ( $N_{in} = \sum_{l=0}^{N_l-1} H_l \times W_l$ ) and hidden dimension of pixel vectors respectively. The computation of MSDeformAttn is shown as:

$$MSDeformAttn(\mathbf{Q}, \mathbf{P}, \mathbf{X}) = \text{Concat}(\mathbf{H}_0, \dots, \mathbf{H}_{N_h-1})$$

$$\text{where } \mathbf{H}_{ij} = \text{Softmax}(\mathbf{Q}_i \mathbf{W}_j^A) \mathbf{V}_j(\mathbf{P}_i + \Delta \mathbf{P}_{ij}) \quad (1)$$

$$\mathbf{V} = \mathbf{X} \mathbf{W}^V, \quad \Delta \mathbf{P} = \mathbf{Q} \mathbf{W}^S$$

where  $\mathbf{Q} \in \mathbb{R}^{N_{in} \times D_{in}}$  and  $\mathbf{V} \in \mathbb{R}^{N_{in} \times D_{in}}$  denote the query matrix and the multi-scale fmaps,  $i$  indexes the row vector in the matrix and  $j$  indexes the  $N_h$  heads.  $\mathbf{W}^A \in \mathbb{R}^{D_{in} \times D_{in}}$ ,  $\mathbf{W}^V \in \mathbb{R}^{D_{in} \times D_{in}}$  and  $\mathbf{W}^S \in \mathbb{R}^{D_{in} \times (2N_h N_l N_p)}$  are all learnable weights, where  $N_p$  denotes the fixed number of sampling points in each level of fmaps.  $\mathbf{H}_{ij} \in \mathbb{R}^{N_{in} \times D_h}$  ( $D_h = D_{in}/N_h$ ) is the  $i^{th}$  row vectors of the output matrix in the  $j^{th}$  attention head.  $\mathbf{P}_i \in \mathbb{R}^{N_{in} \times N_l \times 2}$  enumerates  $N_{in}$  coordinates of regular grids over each level fmap.

Figure 1 (a) illustrates the whole procedure of MSDeformAttn. In each head of MSDeformAttn, the softmax unit normalizes all points in different levels projected from a row vector of the input query and generates the attention probability vector. The MSGS procedure adopts the bilinear interpolation (BI) kernel to process the fractional sampling points and obtains sampling value from the multi-scale fmaps. In the aggregation stage, each pixel vector of the sampling value is multiplied by an element of the attention probability vector and then all the weighted vectors are summed to gain an output vector of a head.

### 2.2 Computational Properties Analysis

As shown in Figure 1 (b), We profile the MSDeformAttn latency breakdown on Deformable DETR [1], DN-DETR [4] and DINO [5] on Nvidia RTX 3090Ti. MSGS and aggregation account for over 60% of the inference runtime of MSDeformAttn, while their computation cost only takes 3.25%, demonstrating severe inefficiency on GPU platforms. This is mainly caused by irregular memory access in MSGS. In MSGS, unbounded sampling coordinates are dynamically generated and incur unpredictable memory access. It violates the locality principles commonly used to reduce DRAM access, resulting in minimal fmap reuse. Moreover, as multi-scale fmaps in MSGS have more pixels than single-scale fmaps, the sampling points are dispersed over a wider range, which further increases memory

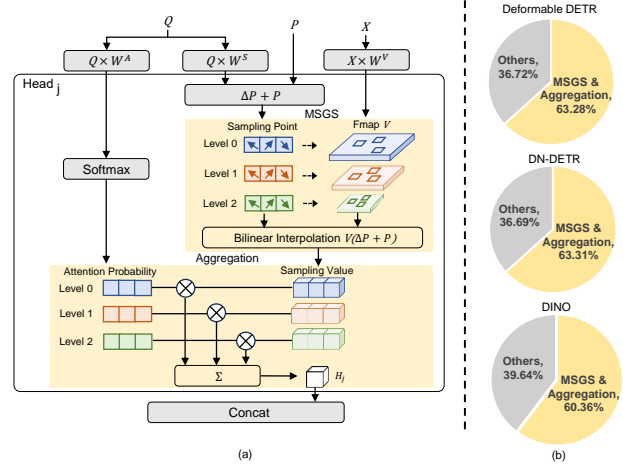


Figure 1: (a) Introduction of MSDeformAttn. (b) MSDeformAttn latency breakdown.

access. In addition, the number of MSGS also grows proportionally with the number of fmap pixels, aggravating the inefficiency of the unordered sampling process.

Although DeformConv also uses a similar grid-sampling module, the workload of MSGS in MSDeformAttn is multiple times higher than DeformConv. In particular, the multi-scale fmaps in MSDeformAttn are 21.3× larger than the single-scale fmaps in DeformConv. Additionally, the sampling points in MSDeformAttn are also  $N_l N_p \times$  more than those in DeformConv in each head. This causes an extremely larger on-chip buffer requirement and more irregular memory access in MSGS.

Existing attention accelerators [11, 10, 12] reduce the computation of weak-related tokens via random projection (ELSA [11]), attention score sort (SpAttn [10]) and approximate computation (BESAPU [12]). However, MSDeformAttn does not explicitly compute token relevance, making their methods inapplicable. Besides, they do not efficiently support the MSGS procedure and lack optimization on the dataflow of MSGS. In MSGS, irregular memory access on multi-scale fmaps requires attention accelerators with up to 9.8MB on-chip buffer size, significantly increasing area and reducing efficiency. DEFA is the first work to exploit sparsity in fmaps and sampling points and to explore the multi-scale parallelism in MSGS processing.

## 3 SPARSITY-AWARE GRID-SAMPLING FOR MSDEFORATTN DATAFLOW

In MSGS, numerous fmap pixels and sampling points cause enormous memory access and have high redundancy. To remove unnecessary memory access and enhance the efficiency of MSGS, we exploit the sparsity in multi-scale fmaps and sampling points via FWP and PAP approaches respectively.

### 3.1 Frequency-Weighted Fmap Pruning

To restrict the size of the large sampled fmaps, we analyze the sampled frequency of each pixel on them and find that it shows a

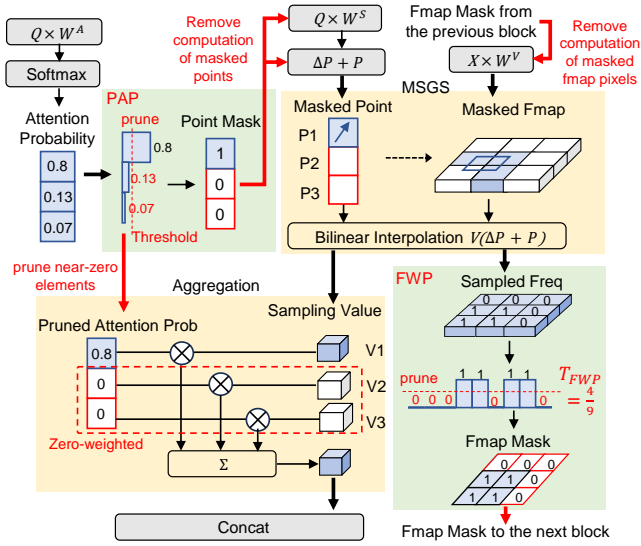


Figure 2: Overview of sparsity-aware grid-sampling.

non-uniform distribution. This demonstrates that a small proportion of pixels has a much higher probability of being accessed and is essential to the detection accuracy. FWP is proposed to remove other unimportant pixels with low sampled frequency. Firstly, the sampled times of every pixel in the fmap are counted in MSGS of the MSDeformAttn block and indicate the sampled frequency. As shown in Figure 2 right, the neighboring points of the sampling point in BI are accessed once, so the sampled frequency of these pixels is counted to 1 and the sampled frequency of the others is 0. Then, the pixels with a lower sampled frequency than the preset threshold are pruned and their locations are recorded in a bit mask as the fmap mask. Finally, the generated fmap mask is applied in the next MSDeformAttn block to eliminate the linear projection and memory access of the masked fmap pixels. Here the threshold in FWP is defined as:

$$T_{FWP} = k \cdot \frac{1}{HW} \sum_{i=0}^{HW-1} F_i \quad (2)$$

where  $k$  is a hyperparameter and  $F_i$  denotes the sampled frequency of the  $i^{th}$  pixel in the fmap of size  $HW$ . In Figure 2 right,  $k$  is assumed as 1 and the fmap size is 9. We adjust  $k$  to achieve a trade-off of accuracy and sparsity in the finetuning.

### 3.2 Probability-Aware Point Pruning

We propose PAP to detect and remove unessential sampling points in MSGS using their related attention probabilities as illustrated in Figure 2 left. In the aggregation process, the sampling values in an attention head are multiplied by the normalized attention probabilities from softmax and then summed up. The summation of attention probabilities is confined to 1 and their differences are exponentially amplified. We set a threshold to filter out the near-zero attention probabilities and they constituted a dominant proportion (over 80% in Deformable DETR). The sampling values weighted by them make small contributions to the results of aggregation and

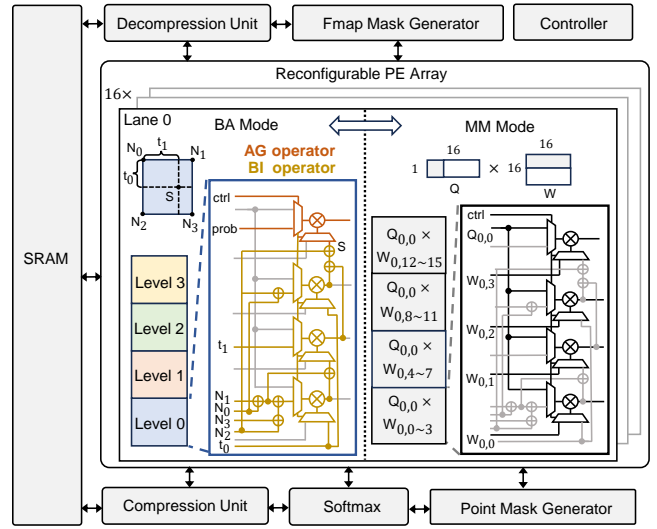


Figure 3: Overview of DEFA architecture.

detection accuracy. Hence, the near-zero attention probabilities are pruned and the point mask is established as a bit mask to eliminate the following processing of the sampling points generating the following processing of the sampling points generating the current MSDeformAttn block. In Figure 2 left, the zero-weighted sampling values  $V_2, V_3$  are multiplied with 0 in the aggregation process after PAP, and thereby the sampling points  $P_2, P_3$  producing  $V_2, V_3$  are unnecessary and removed to save computation cost and memory access.

## 4 HIGH-THROUGHPUT DEFORMABLE ATTENTION ARCHITECTURE

In this section, we present DEFA architecture co-designed with the pruning algorithms to efficiently process MSDeformAttn in Figure 3. The fmap mask generator and sampling point mask generator implement FWP and PAP, respectively. The compression unit decompression unit eliminates the redundant bandwidth and computation of the masked data. The reconfigurable PE array can switch between the matrix multiplication (MM) mode and the BI mode to accelerate MM or fine-grained operator fusion.

### 4.1 Dataflow Overview

DEFA rearranges the operators in MSDeformAttn to enable the application of FWP and PAP, reducing computation and memory access. Firstly, attention probabilities are calculated and the point mask is updated. Then, the masked sampling points pruned by the point mask are generated in the reconfigurable PE array in the MM mode, which includes  $\Delta P = QW^S$  in Eq.1. Next, the linear projection of the masked fmaps ( $V = XW^V$  in Eq.1) is pruned by the fmap mask from the last MSDeformAttn block and performed in the PE array. Finally, DEFA processes the fused MSGS and aggregation operators with the reconfigurable PE array in the BA mode. Meanwhile, the fmap mask generator receives the sampling address in the BI and executes FWP for the next block.

Inspired by the prior work on DeformConv [13], we propose the level-wise range-narrowing scheme to decrease on-chip storage in

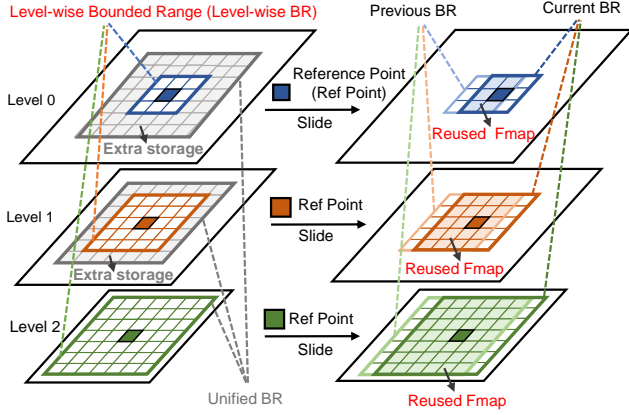


Figure 4: Level-wise range-narrowing scheme.

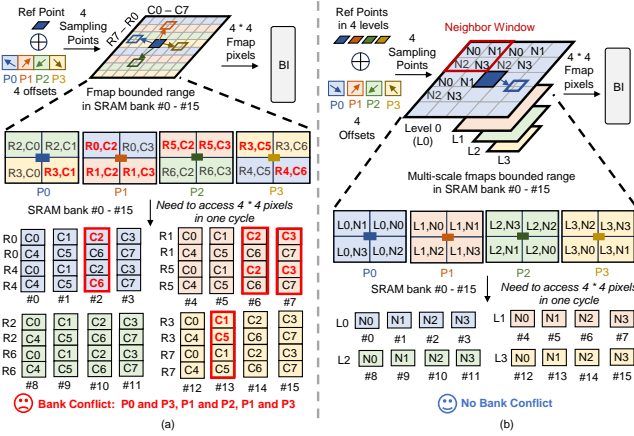


Figure 5: Illustration of (a) intra-level parallel processing and (b) inter-level parallel processing.

MSGs, as illustrated in Figure 4 left. DEFA uses bounded ranges of different sizes to limit the sampling offsets around a reference point based on the level of multi-scale fmaps. This is because the bounded range in some levels can be further reduced without any accuracy loss. Applying unified restriction on all levels of the multi-scale fmaps causes an extra 25% storage requirement. Figure 4 right shows that when the reference point slides to the next pixel in fmaps, the overlapping pixels between the previous and the current bounded range are reused to avoid repetitive memory access.

## 4.2 Multi-Scale Parallel Processing

To minimize latency and optimize hardware resource utilization, we investigate both intra-level and inter-level parallel processing in MSGs. The purpose of DEFA in the BI of MSGs is to calculate four sampling points in parallel without bank conflicts. This requires accessing 16 fmap pixels, with four neighboring pixels for each sampling point, from 16 SRAM banks in one cycle. If DEFA processes four sampling points in one level of multi-scale fmaps, which is intra-level parallel processing presented in Figure 5(a), all the pixels within the bounded range centered on the reference

point are stored in the SRAM. This can cause bank conflicts when multiple sampled pixels are stored in the same bank. To prevent this issue, we propose inter-level parallel processing based on the observation that sampling points are only located in the same level of multi-scale fmaps as their reference points, which is utilized to limit the sampling range in their level. As illustrated in Figure 5(b), compared to intra-level parallel processing, DEFA processes four sampling points extended from the reference points in four levels of multi-scale fmaps. In addition, the pixels within the bounded range of every level are stored in every four banks of the overall 16 SRAM banks. The bounded range is tiled into several *Neighbor Windows*, and the four pixels in each *Neighbor Window* are mapped to the four SRAM banks. This approach allows for the sampled pixels to be accessed in different banks without any bank conflicts.

## 4.3 Fine-Grained Operator Fusion with the Reconfigurable PE Array

We propose fine-grained operator fusion of MSGs and aggregation, removing the off-chip transfer of sampling value. To support the process with the limited computing resources in the PE array, we transform BI and design a reconfigurable PE array alternating between the BA mode and the MM mode, as shown in Figure 3. Assume there is a sampling point, denoted as  $S$  at  $(x, y)$ , with four neighboring points denoted as  $N_0$  at  $(x_0, y_0)$  (top left),  $N_1$  at  $(x_1, y_0)$  (top right),  $N_2$  at  $(x_0, y_1)$  (bottom left) and  $N_3$  at  $(x_1, y_1)$  (bottom right) respectively. Then BI is implemented as:

$$S = N_0(x_1 - x)(y_1 - y) + N_1(x - x_0)(y_1 - y) + N_2(x_1 - x)(y - y_0) + N_3(x - x_0)(y - y_0) \quad (3)$$

As the coordinates of the four neighboring points are all integers and located at the four corners of the grid,  $x_1$  and  $y_1$  are equal to  $x_0 + 1$  and  $y_0 + 1$  respectively. After replacing them and a series of transformations, Eq.3 becomes:

$$S = N_0 + (N_2 - N_0)t_0 + [(N_1 - N_0) + (N_3 - N_2 - N_1 + N_0)t_1]t_1 \quad (4)$$

Where  $t_0 = y - y_0$  and  $t_1 = x - x_0$ . The calculation of  $t_0$  and  $t_1$  is performed in other units. As a result, the BI operator part in Figure 3 only employs three multipliers and seven adders. The AG operator part performs the multiplication of attention probability and  $S$ . Additionally, the PE array in the MM mode conducts MM between a 16-element vector ( $Q$ ) and a  $16 \times 16$  tile ( $W$ ) in the output-stationary dataflow.

## 5 EVALUATION

### 5.1 Experimental Methodology

**5.1.1 Benchmarks.** We evaluate DEFA on MSDeformAttn layers in the encoders of Deformable DETR (De DETR) [1], DN-DETR [4] and DINO [5]. The evaluation task is object detection on the COCO 2017 dataset [15]. We utilize PyTorch to conduct experiments on the benchmarks with reference to the official implementation. Fine-tuning is applied to the modified models by the software methods in Section 3 to recover the accuracy. The MSDeformAttn modules in the encoder layers of the models are quantized to 12bits during the inference. We compare DEFA with NVIDIA RTX 2080Ti and 3090Ti GPUs and SOTA attention accelerators [11, 10, 12].

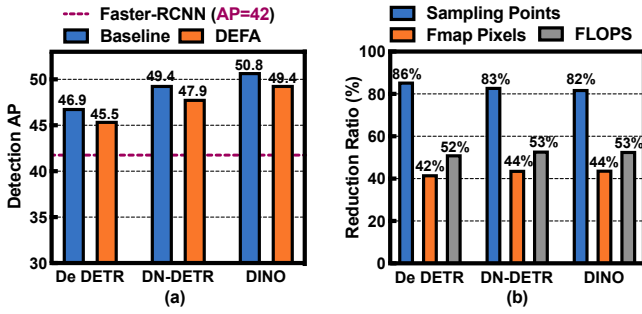


Figure 6: (a) Detection Average Precision of our methods and comparisons with other works. (b) Reduction in sampling points, fmap pixels, and computation cost.

5.1.2 *Hardware Implementation.* DEFA is described in SystemVerilog and synthesized with Synopsys Design Compiler for 400MHz clock frequency to estimate the area and power under a 40nm technology. We implement a cycle-accurate simulator to model the computation and memory access and evaluate the performance of DEFA. We obtain the area and energy consumption of SRAM with CACTI [16], and a moderate 256GB/s HBM2 is used as the external memory system, consuming 1.2pJ/b [17] for data access.

## 5.2 Algorithm Evaluation

Figure 6 (a) presents the standard average precision (AP) of our methods and comparisons with the baseline of the benchmarks as well as the Faster R-CNN [9]. The processing of FWP, PAP, level-wise range-narrowing, and INT12 quantization causes 0.8, 0.3, 0.26, and 0.07 AP drop on average on the benchmarks, respectively. Compared to INT12 quantization, INT8 quantization is not adopted because it results in an average drop of 9.7 AP on the benchmarks, which is an unacceptable accuracy degradation. DEFA preserves a relatively high detection accuracy with negligible AP loss, which is 3.5-7.4 AP higher than Faster R-CNN. Figure 6 (b) shows the reduction ratio in sampling points, fmap pixels, and computation cost achieved by our pruning algorithms. FWP and PAP reduce 43% fmap pixels and 84% sampling points on average, and the computation cost on the unimportant fmap pixels and sampling points is also eliminated, accounting for more than 50% of the overall computation. For level-wise range-narrowing, we adjust bounded ranges of sampling offsets in each level to achieve a trade-off between accuracy and SRAM size.

## 5.3 Performance Gain from Our Hardware Optimization Tactics

5.3.1 *Multi-scale Parallel Processing.* Figure 7 (a) indicates the MSGS throughput improvement of inter-level parallel processing over intra-level parallel processing on the selected benchmarks. The bank conflicts are detected in intra-level parallel processing when plural sampling points need to access different addresses in the same SRAM bank in one clock cycle. In this case, extra clock cycles are spent on detecting bank conflicts, stopping the pipeline, and sequentially processing the requests. The proposed inter-level parallel processing completely avoids bank conflicts and achieves 3.06x

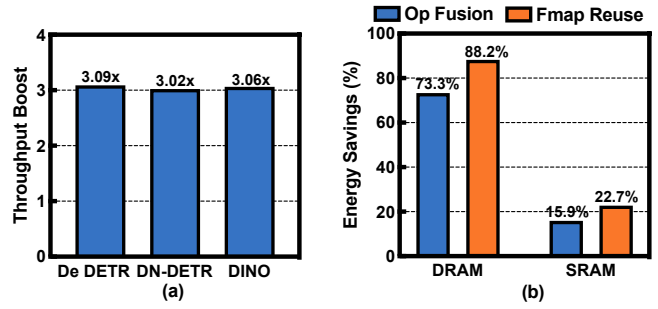


Figure 7: (a) MSGS throughput boost of inter-level parallel processing over intra-level parallel processing. (b) Energy savings of fine-grained operator fusion and fmap reuse.

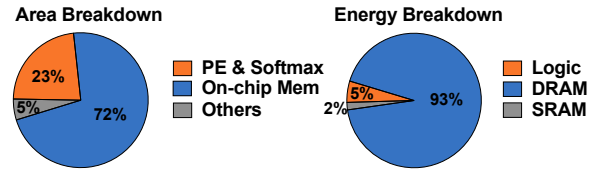


Figure 8: Area breakdown and energy breakdown of DEFA.

higher MSGS throughput than the intra-level parallel processing on average under the same degree of parallelism.

5.3.2 *Fine-grained Operator Fusion.* As shown in Figure 7 (b), fine-grained operator fusion (op fusion) of MSGS and aggregation results in 73.3% and 15.9% energy saving on DRAM access and SRAM access of the overall MSGS energy consumption in memory access. Fine-grained operator fusion reduces the off-chip transfer of the BI result and utilizes the BI result directly to compute aggregation in the reconfigurable PE array in the BA mode, avoiding SRAM access. DEFA only adds 0.5% extra SRAM storage to support fine-grained operator fusion.

5.3.3 *Fmap Reuse.* Figure 7 (b) presents the energy saving of fmap reuse. Fmap reuse significantly reduces DRAM access of the fmap pixels in the overlapping bounded range, saving 88.2% of the total MSGS energy consumption in memory access. The writing operations to the SRAM of the repetitive fmap pixels fetched from the DRAM are also eliminated, which reduces 22.7% energy consumption of the overall MSGS energy consumption in memory access.

## 5.4 Comparisons with Other Platforms

We compare the speedup and the energy efficiency (EE) improvement of DEFA with the Nvidia GPUs in Figure 9. The performances of CPUs are not evaluated because MSDeformAttn only has a CUDA implementation. During the comparison with GPUs, we scale up DEFA to attain 13.3 TOPS and 40 TOPS peak throughput respectively, which matches Nvidia 2080Ti (13.5 TFLOPS@FP32) GPU and Nvidia 3090Ti (40 TFLOPS@FP32) GPU. DEFA achieves 10.1-31.9x speedup as well as 20.3-37.7x energy efficiency improvement over Nvidia 2080Ti GPU (250W) & Nvidia 3090Ti GPU (450W) on average. The high speedup results from the inter-level parallel

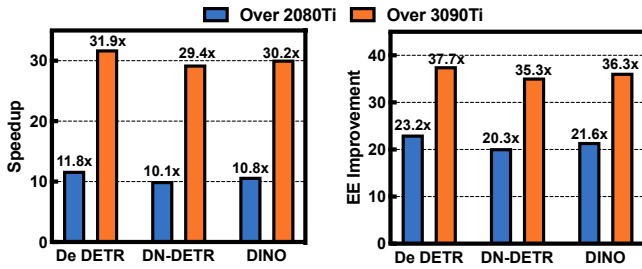


Figure 9: Speedup and energy Efficiency improvement of DEFA over GPUs.

processing without any bank conflicts in MSGS. DEFA further accelerates MSDeformAttn via FWP and PAP reducing the computation of redundant fmap pixels and sampling points. The energy saving is attributed to DRAM and SRAM access reduction through fine-grained operator fusion and fmap reuse. Figure 8 shows the area and energy breakdown of DEFA. The SRAM occupies the largest area since MSGS requires a large amount of on-chip memory to store multi-level fmaps. The DRAM access dominates the energy consumption due to the large data transfer in MM.

Table 1 compares DEFA and other attention asic platforms [11, 10, 12]. DEFA achieves 3.7 $\times$ , 3.4 $\times$  and 2.2 $\times$  higher energy efficiency than ELSA [11], SpAtten [10] and BESAPU [12] for the following reasons. ELSA prefetches the key matrix and speculates candidates for every query token through orthogonal projection before attention computation. Its preprocessing needs to access the query and key matrix in SRAM numerous times and consumes large power, while the SRAM access of the pruning processing in DEFA takes less than 0.1% of the overall SRAM access and the pruning process in DEFA consumes extremely less power. SpAtten structurally removes the attention tokens and heads with low cumulative scores. Compared to the coarse-grained pruning methods in SpAtten, DEFA performs fine-grained FWP and PAP on fmap pixels and sampling points. Therefore, DEFA attains a higher pruning ratio with acceptable AP loss, which saves more computation and energy than SpAtten. BESAPU bidirectionally speculates and approximately computes weakly related tokens with an out-of-order scheduler to save energy consumption. However, the improvement of the energy efficiency resulting from the approximate computation highly depends on the ratio of weakly related tokens, which denotes the sparsity of attention, because the complex control logic consumes large energy. In contrast, fine-grained operator fusion and fmap reuse can save a large amount of memory access to enhance energy efficiency in MSGS without the restriction of sparsity. Besides, the speculation in BESAPU only reduces the negative operations of weakly related tokens, while FWP and PAP in DEFA can remove all the computation of the redundant fmap pixels and sampling points, thus saving more energy. Hence, DEFA achieves higher energy efficiency than BESAPU.

## 6 CONCLUSION

We propose DEFA, the first algorithm-architecture co-design for efficient MSDeformAttn acceleration. On the algorithm level, we

Table 1: Comparison with Other ASIC Platforms

	[11] ISCA'21	[10] HPCA'21	[12] JSSC'22	DEFA
Function	Attention			Deform Attn
Technology(nm)	40	40	28	40
Area(mm <sup>2</sup> )	1.26	1.55	6.82	2.63
Frequency(MHz)	1000	1000	500	400
Precision	INT9	INT12	INT12	INT12
Power(mW)	969.4	294.0	272.8	99.8
Throughput(GOPS)	1088	360	522	418
Energy Effi.(GOPS/W)	1120	1224	1910	4187

present FWP and PAP to effectively prune the fmap pixels and sampling points in MSGS so that the memory access and computation are significantly reduced. On the architecture level, DEFA adopts inter-level parallel processing for throughput enhancement. DEFA further utilizes fine-grained operator fusion and fmap reuse to alleviate memory footprint. DEFA achieves speedup and energy saving over Nvidia RTX 2080Ti and 3090Ti, and higher energy efficiency than the SOTA attention accelerators.

## ACKNOWLEDGMENTS

This work was supported by the National Natural Science Foundation of China under Grant 62074097.

## REFERENCES

- [1] Xizhou Zhu et al. 2021. Deformable DETR: Deformable Transformers for End-to-End Object Detection. In *ICLR*.
- [2] Jifeng Dai et al. 2017. Deformable Convolutional Networks. In *ICCV*, 764–773.
- [3] Nicolas Carion et al. 2020. End-to-End Object Detection with Transformers. In *ECCV*, 213–229.
- [4] Feng Li et al. 2022. DN-DETR: Accelerate DETR Training by Introducing Query Denoising. In *CVPR*, 13619–13627.
- [5] Hao Zhang et al. 2022. DINO: DETR with Improved DeNoising Anchor Boxes for End-to-End Object Detection. In *ICLR*.
- [6] Zhiqi Li et al. 2022. BEVFormer: Learning Bird’s-Eye-View Representation from Multi-Camera Images via Spatiotemporal Transformers. In *ECCV*, 1–18.
- [7] Yiming Li et al. 2023. VoxFormer: Sparse Voxel Transformer for Camera-based 3D Semantic Scene Completion. In *CVPR*, 9087–9098.
- [8] Yuanhui Huang et al. 2023. Tri-Perspective View for Vision-Based 3D Semantic Occupancy Prediction. In *CVPR*, 9223–9232.
- [9] Shaoqing Ren et al. 2015. Faster R-CNN: Towards Real-Time Object Detection with Region Proposal Networks. *NeurIPS*, 28.
- [10] Hanrui Wang et al. 2021. SpAtten: Efficient Sparse Attention Architecture with Cascade Token and Head Pruning. In *HPCA*, 97–110.
- [11] Tae Jun Ham et al. 2021. ELSA: Hardware-software co-design for efficient, lightweight self-attention mechanism in neural networks. In *ISCA*, 692–705.
- [12] Yang Wang et al. 2022. An Energy-Efficient Transformer Processor Exploiting Dynamic Weak Relevances in Global Attention. *IEEE JSSC*, 58, 1, 227–242.
- [13] Qijing Huang et al. 2021. CoDeNet: Efficient Deployment of Input-Adaptive Object Detection on Embedded FPGAs. In *FPGA*, 206–216.
- [14] Shan Li et al. 2022. A Computational-Efficient Deformable Convolution Network Accelerator via Hardware and Algorithm Co-Optimization. In *SiPS*, 1–6.
- [15] Tsung-Yi Lin et al. 2014. Microsoft COCO: Common Objects in Context. In *ECCV*, 740–755.
- [16] Naveen Muralimanohar, Rajeev Balasubramanian, and Norman P Jouppi. 2009. CACTI 6.0: A tool to model large caches. *HP laboratories*, 27, 28.
- [17] Soroush Ghodrati et al. 2020. Bit-parallel vector composability for neural acceleration. In *DAC*, 1–6.